in preparation for departure. Moreover, the protein-for-water strategy may be unique to uricotelic animals, which dispose of nitrogenous wastes with minimal associated water losses. Migrating bats, for example, may show very different responses to water stress than birds.

Our findings will be useful for the modification of existing bird flight range models by incorporating the effects of atmospheric conditions on fuel mixture, which provides new insight regarding the limits to migratory flight. We have shown that ambient conditions experienced aloft can affect the composition of metabolic fuels used in flight, which may then influence flight range or overall pace of migration. Higher average temperatures in flight could potentially increase water losses and require birds to stop prematurely or to catabolize more protein. Additional time at stopover could then be required to replenish excess protein catabolized in flight.

References and Notes

1. L. Jenni, S. Jenni-Eiermann, *J. Avian Biol.* **29**, 521 (1998).
2. P. F. Battley *et al.*, *Proc. R. Soc. London B Biol. Sci.* **267**, 191 (2000).
3. U. Bauchinger, S. R. McWilliams, *Physiol. Biochem. Zool.* **82**, 787 (2009).
4. Å. Lindström, A. Kvist, T. Piersma, A. Dekinga, M. W. Dietz, *J. Exp. Biol.* **203**, 913 (2000).
5. C. J. Pennycuick, *J. Theor. Biol.* **191**, 47 (1998).
6. R. Schwilch, A. Grattarola, F. Spina, L. Jenni, *J. Exp. Biol.* **205**, 687 (2002).
7. M. Klaassen, *J. Avian Biol.* **35**, 4 (2004).
8. I. Giladi, B. Pinshow, *J. Comp. Physiol. B* **169**, 311 (1999).
9. S. Engel, H. Biebach, G. H. Visser, *Physiol. Biochem. Zool.* **79**, 763 (2006).
10. N. Carmi, B. Pinshow, W. Porter, J. Jaeger, *Auk* **109**, 268 (1992).
11. R. E. Gill, T. Piersma, G. Hufford, R. Servranckx, A. Riegen, *Condor* **107**, 1 (2005).
12. B. J. Stutchbury *et al.*, *Science* **323**, 896 (2009).
13. H. Biebach, in *Bird Migration: Physiology and Ecophysiology*, E. Gwinner, Ed. (Springer-Verlag, Berlin, 1990), pp. 352–367.
14. M. M. Landys, T. Piersma, G. H. Visser, J. Jukema, A. Wijker, *Condor* **102**, 645 (2000).
15. H. Schmaljohann, B. Bruderer, F. Liechti, *Anim. Behav.* **76**, 1133 (2008).
16. C. G. Guglielmo, L. P. McGuire, A. R. Gerson, C. L. Seewagen, *J. Ornithol.* **152** (suppl. 1), S75 (2011).
17. For further description of the wind tunnel and detailed experimental methods and statistical analysis, see the supporting online material on *Science* Online.
18. R. T. Holmes, R. H. Sawyer, *Comp. Biochem. Physiol. A* **50**, 527 (1975).
19. J. R. B. Lighton, in *Measuring Metabolic Rates* (Oxford Univ. Press, New York, 2008), pp. 105–123.
20. M. Wikelski *et al.*, *Nature* **423**, 704 (2003).
21. I. Giladi, D. L. Goldstein, B. Pinshow, R. Gerstberger, *J. Exp. Biol.* **200**, 3203 (1997).
22. A. R. Gerson, C. G. Guglielmo, *Am. J. Physiol. Regul. Integr. Comp. Physiol.* **300**, R925 (2011).
23. S. R. McWilliams, W. H. Karasov, *Comp. Biochem. Physiol. A* **128**, 579 (2001).
24. U. Bauchinger, A. Wohlmann, H. Biebach, *Zoology* **108**, 97 (2005).
25. M. Klaassen, *J. Exp. Biol.* **199**, 57 (1996).
26. M. Klaassen, A. Kvist, A. Lindstrom, *Condor* **102**, 444 (2000).
27. C. L. Seewagen, C. G. Guglielmo, *J. Comp. Physiol. B* **181**, 413 (2011).
28. H. Schmaljohann, F. Liechti, B. Bruderer, *Behav. Ecol. Sociobiol.* **63**, 1609 (2009).
29. H. Biebach, *J. Avian Biol.* **29**, 529 (1998).

Acknowledgments: We thank W. Bezner-Kerr for technical assistance with wind tunnel operations; M. Rebuli, T. Farrell, B. Kriengwatana, and A. Macmillan for assistance with animal care; Y. Morbey and L. McGuire for expert statistical advice; A. Boyle, T. Crewe, L. Kennedy, B. McCabe, S. Nebel, E. Price, B. Thurber, and M. Gerson for assistance or advice during this project; and P. Taylor, J. McCracken, S. Mackenzie, M. Burrell, and the volunteers at the Long Point Bird Observatory for their assistance. A.R.G. was supported by an Natural Sciences and Engineering Research Council of Canada (NSERC) Alexander Graham Bell Canada Graduate Scholarship. This study was funded by an NSERC Discovery Grant and by Leaders Opportunity and New Initiatives grants from the Canada Foundation for Innovation and Ontario Research Fund to C.G.G. and colleagues.

Supporting Online Material

www.sciencemag.org/cgi/content/full/333/6048/1434/DC1
Materials and Methods
Tables S1 and S2
References (*30*–*33*)

28 June 2011; accepted 14 July 2011
10.1126/science.1210449

Generation of Spatial Patterns Through Cell Polarity Switching

Sarah Robinson,[1] Pierre Barbier de Reuille,[2] Jordi Chan,[1] Dominique Bergmann,[3] Przemyslaw Prusinkiewicz,[4] Enrico Coen[1]*

The mechanisms that generate dynamic spatial patterns within proliferating tissues are poorly understood, largely because of difficulties in unravelling interactions between cell specification, polarity, asymmetric division, rearrangements, and growth. We address this problem for stomatal spacing in plants, which offer the simplifying advantage that cells do not rearrange. By tracking lineages and gene activities over extended periods, we show that limited stem cell behavior of stomatal precursors depends on maintenance of the SPEECHLESS (SPCH) transcription factor in single daughter cells. Modeling shows how this property can lead to observed stereotypical stomata lineages through a postmitotic polarity-switching mechanism. The model predicts the location of a polarity determinant BASL over multiple divisions, which we validate experimentally. Our results highlight the dynamic two-way interactions between stem cells and their neighborhood during developmental patterning.

Mature leaves of *Arabidopsis* contain numerous stomata interspersed with non-stomatal cells (*1*). Stomata derive from precursors (meristemoids) that may undergo several rounds of asymmetric division during which only one daughter retains meristemoid identity, suggesting that they behave as stem cells for a limited period (*2*, *3*). Meristemoids eventually differentiate into guard mother cells (GMCs), which in turn produce the two guard cells surrounding the stomatal pore. The molecular genetic and cellular control of many of these steps has been extensively analyzed (*4*–*10*). However, it is still unclear how initial stomatal lineage patterns are generated. This is because previous studies have only imaged gene expression at particular time points or followed lineages after many stomata have already formed.

To understand how stomatal patterning occurs, we used live confocal imaging methods to track growing leaves expressing various markers from precursor initiation to differentiation. We first tracked a plasma membrane green fluorescent protein (GFP) marker line to determine early lineage patterns. Retrospective analysis of the tracking data was used to classify cells that went on to produce GMCs. A cell that included a single GMC descendant during the period of imaging was termed a precursor cell or P cell, whereas all other cells were called N cells. We tracked 50 lineages distributed across the leaf blade. The results showed that P cells behave as stem cells for three or four rounds of division, after which they become GMCs (Fig. 1A and fig. S7).

P cells exhibit several properties that distinguish them from N cells. P cells divide more often than N cells and become progressively smaller through division. The reduction in size is partly because P cells divide asymmetrically, with the smaller cell usually retaining P cell identity and being 39% of the parent cell size on average (fig. S1). Reduction in P cell size is also enhanced by P cells tending to divide at successively smaller sizes (Fig. 1C). N cells may also divide, but such divisions are usually symmetric and occur when N cells reach more than twice their birth size (fig. S2). In some cases, N cells produce daughters that divide asymmetrically at less than twice their birth size, suggesting these N cells have reacquired P identity (Fig. 1B and fig. S3, pink).

[1]John Innes Centre, Norwich Research Park, Colney, Norwich NR4 7UH, UK. [2]University of East Anglia, Norwich NR4 7TJ, UK. [3]371 Serra Mall, Stanford University, Stanford, CA 94305–5020, USA. [4]Department of Computer Science, University of Calgary, 2500 University Drive NW, Calgary, Alberta T2N 1N4, Canada.

*To whom correspondence should be addressed. E-mail: enrico.coen@jic.ac.uk

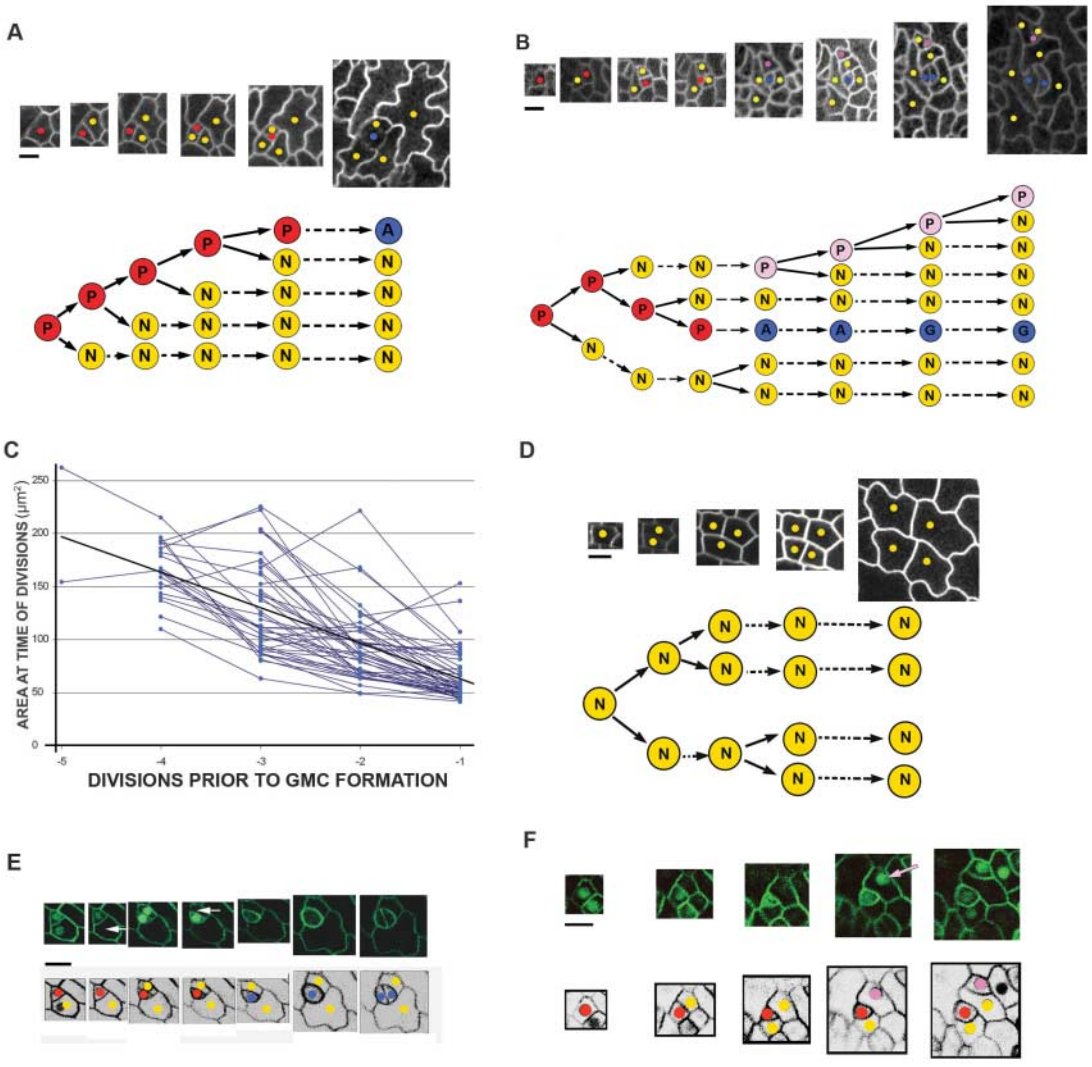

Fig. 1. Fate and specification of stomatal precursors. (**A**) A tracked lineage showing P cells (red), GMC cells (A, blue), and N cells (yellow). Times of image capture (to the nearest hour) from left to right are 00 hours, 04 hours, 20 hours, 33 hours, 47 hours, and 92 hours. The pedigree is shown below. (**B**) A lineage in which one N cell appears to regain P identity (pink). Guard cells (G) are indicated with blue. Times of image capture (to the nearest hour) from left to right are 00 hours, 12 hours, 21 hours, 33 hours, 45 hours, 50 hours, 63 hours, and 83 hours. (**C**) Area at which P cells divide declines over successive divisions before GMC formation. (**D**) *spch* mutant lineages only include N cells and show even bifurcations. (**E**) Tracking GFP-labeled SPCH protein shows that it disappears in N daughter cells (white arrows) a few hours after division. Times of image capture (to the nearest hour) from left to right are 00 hours, 02 hours, 25 hours, 27 hours, 48 hours, 73 hours, and 75 hours. (**F**) Tracking GFP-labeled SPCH protein shows that N cells that reacquire SPCH (pink arrow) also regain P identity (pink dot). Times of image capture from left to right are 00 hours, 04 hours, 19 hours, 32 hours, 47 hours, and 92 hours. Scale bars (black line) indicate 10 μm.

As well as showing limited stem cell behavior, stomatal lineages also exhibit stereotypical patterns of division (Fig. 2 and fig. S7). The most common pattern is for P cells to undergo two or three rounds of division in alternating orientations, followed by a division across adjacent walls, creating a spiral arrangement with an internalized P cell (Figs. 1, A and B, 2, A and B, and fig. S7, A and B). The second pattern is similar except that two successive divisions span adjacent walls (Fig. 2, C and D, and fig. S7C). The third and least common pattern involves a parallel rather than alternating division (Fig. 2, E and F, and fig. S7D). Lineages in which the P cell was not internalized were largely truncated versions of these arrangements (fig. S8). Any model for stomatal patterning therefore needs to account for both the stem cell behavior of P cells and the stereotypical manner in which they divide.

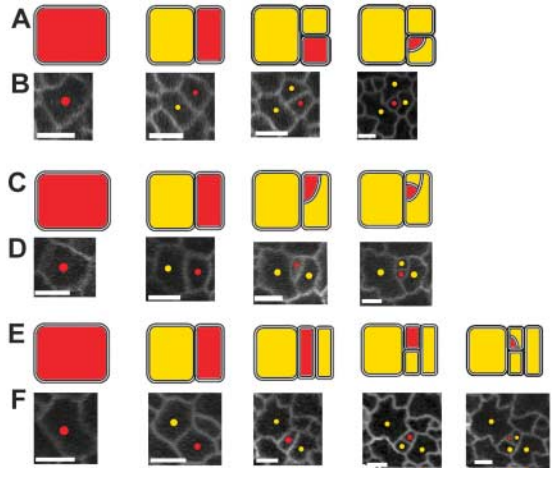

Fig. 2. Patterns observed among lineages involving more than two rounds of division (47 lineages analyzed). Interpretive diagrams (A, C, and E) are shown above time-lapse confocal images (B, D, and F). Red, P cells; yellow, N cells; scale bars (white lines), 10 μm. (**A** and **B**) P cell undergoes two or three divisions in alternating orientations, followed by a division across adjacent walls (21 lineages). The result is a spiral arrangement. (**C** and **D**) As in (A) and (B) except that two successive divisions span adjacent walls (10 lineages). (**E** and **F**) Two parallel divisions before an alternating division and then a final division that joins adjacent walls (3 lineages). The remaining 13 lineages corresponded to truncated versions of the above three patterns.

To account for stem cell property of P cells, we hypothesized that they express an identity factor that is only maintained in a single daughter after division, allowing it to retain P cell identity. A good candidate gene for this factor is *SPEECHLESS* (*SPCH*). *SPCH* encodes a basic helix-loop-helix transcription factor that is required for the formation of stomatal lineages and is also able to drive stomatal development when activated ectopically (*4*). SPCH protein is found in a subset of epidermal cells, often adjacent to each other, and is restricted to smaller cells in older leaves (*4*). Although maintenance of SPCH in single daughters is consistent with these observations, this conclusion was not previously

drawn, perhaps because of difficulty in inferring such a behavior from static images. We therefore tracked leaves containing a functional *SPCH::SPCH-GFP* protein fusion for extended periods to determine its spatiotemporal dynamics. SPCH protein was detected in P cells and in both daughters immediately after P division, accounting for the observation that SPCH is often found in adjacent cells (Fig. 1E and fig. S4). However, a few hours after division, SPCH protein was no longer seen in the N daughter cell, whereas it was maintained in the P daughter (Fig. 1E and fig. S4). This pattern of maintenance in single daughters continued through successive rounds of division until formation of the GMC, when SPCH expression was extinguished. These results therefore support the hypothesis that P identity is maintained in single daughters and show that this identity is probably mediated by SPCH activity.

This model predicts that SPCH should be reactivated in N cells that regain P identity. Live imaging of the *SPCH-GFP* line showed that some N cells regain SPCH protein expression at later stages. After regaining SPCH signal, these cells behave as P cells: dividing asymmetrically with SPCH activity being maintained in a single daughter cell (Fig. 1F and fig. S5, A and C). Thus, cells that regain SPCH activity also regain P identity. As well as being reactivated in these early lineages, SPCH could also be reactivated at later stages of development in cells neighboring stomata, giving rise to secondary stomata (*3*) (fig. S5, E and G). A further prediction of the model is that cells in a *spch* mutant leaf should behave as N cells. Consistent with this prediction, tracking *spch* mutant leaves revealed bifurcating rather than stem cell lineages, and daughter cells that divided when they reached more than twice their birth size, typical of N cells (Fig. 1D and fig. S6).

Having established that P cell identity is likely maintained in single daughters through SPCH, we extended our model to investigate how P cells divide asymmetrically and become surrounded by their N cell relatives. A key gene involved in controlling asymmetric division of stomatal precursors is *BASL* (*11*). BASL protein is localized to the nucleus and to a peripheral region of the cell; the peripheral pool is highly polarized, sufficient for BASL function, and inherited by the larger daughter cell after division (*11*). The smaller daughter may regain peripheral BASL expression, which again marks a region that will belong to the larger daughter after the next division. Although these results show that peripheral BASL acts as a polarity marker for an individual asymmetric division, it is unclear how BASL's peripheral location and/or polarizing activity operates during consecutive divisions or how this process is related to the observed stereotypical division patterns.

To incorporate BASL in our model, we first considered a simplified case of a growing one-dimensional file generated by dividing P cells. Two basic patterns can arise depending on how BASL is positioned over multiple division rounds.

In one case, peripheral BASL is localized near the new division boundary after division. This rule leads to a lineage with an apical P cell (Fig. 3A) and is formally equivalent to a variety of plant and animal stem cells in which stem cell identity is maintained at one end (*12*, *13*).

Another possibility is that the peripheral BASL is localized away from the new division boundary (Fig. 3B) (*14*). In this case, polarity of the daughter is opposite to that of the mother, so we call this pattern postmitotic polarity switching. Positioning of BASL may be determined through either a signal from the new boundary, as in yeast (*15*, *16*), or an inhibitory signal from the recent non–stem cell neighbor (Fig. 3B, orange). Successive application of the postmitotic polarity-switching rule leads to internalization of the P cell, consistent with the observed stomatal lineages.

To determine whether polarity switching could account for the observed stereotypical stomatal lineage patterns, we extended our model to two dimensions. This extension required a rule for determining the position and orientation of new division walls. In accordance with previous studies, cells were divided by walls taking the shortest path across the cell passing through the nucleus, initially assumed to be at the cell center (*17*, *18*) (Fig. 3C). Asymmetric divisions could then be implemented by displacing the nucleus away from the center of the cell. We found that small displacements result in geometrically asymmetric divisions (Fig. 3D), whereas larger displacements produce triangular cells (Fig. 3E), a feature exhibited by P cells during later division rounds (Fig. 2 and fig. S7). A postmitotic polarity switch was then incorporated by hypothesizing that BASL protein becomes localized in the cell periphery at a position furthest

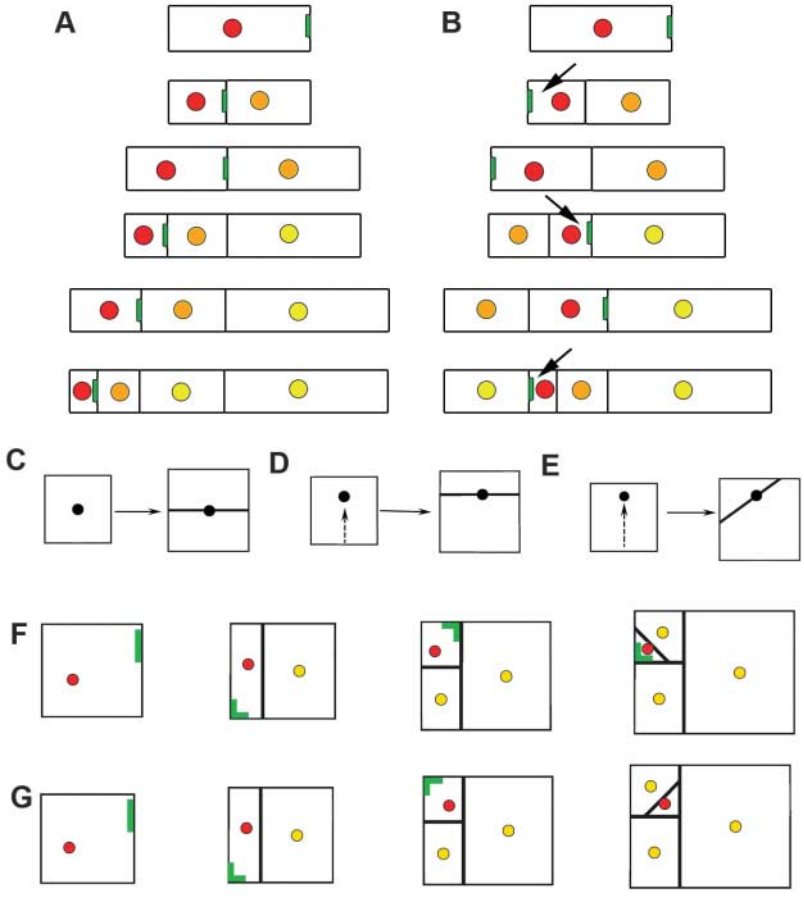

Fig. 3. Models for P cell lineages. (**A** and **B**) One-dimensional lineage models. (A) Peripheral BASL (green) in a mother P cell (red) marks a region that will belong to the N cell daughter (orange) after division. Peripheral BASL in the new P cell becomes localized to the division boundary, next to the recently produced N cell (orange). Reiteration of this rule leads to a file of cells with an apical P cell (older N cells shown in yellow). (B) Postmitotic polarity-switching mechanism in which BASL relocates away from the new division boundary after each division (arrows), leading to internalization of the P cell. (**C**) Dividing a square cell through its center produces a symmetric division. (**D**) Slight displacement of the nucleus (arrow) results in an asymmetric division. (**E**) Larger nuclear displacement results in an asymmetric division and the generation of a triangular cell. (**F**) For growth in two dimensions, if peripheral BASL is localized far from the newest division wall (or neighbor), the P cell need not be internalized. (**G**) If peripheral BASL is localized far from all new walls (*19*), the P cell is internalized. This lineage pattern corresponds to that shown in Fig. 2, A and B.

removed from the newest wall after P cell division. This model did not consistently lead to internalization of P cells (Fig. 3F). To address this problem, we explored a second model in which peripheral BASL becomes localized at a position furthest removed from all recent division walls (*19*) (i.e., all division walls formed after the establishment of P cell identity in the initial cell). This model generated internalized P cells (Fig. 3G).

To determine whether the second model could account for all observed lineage patterns (Fig. 2), we varied the initial cell geometry, anisotropy of growth, and extent to which the nucleus is displaced away from peripheral BASL. This parameter search showed that all experimentally observed patterns could be generated by the model (Figs. 3G and 4, A and B).

As a further test of the model, we tracked the position of BASL in P cell lineages over multiple rounds of division (Fig. 4, C, F, and I, and figs. S9 and S10). In accordance with previous studies (*11*), peripheral BASL always marked the region that will belong to the N cell in the next division. From the cell outlines and sequence of divisions, we computed the position furthest from recent division walls, corresponding to the position of peripheral BASL predicted by the model. In 13 out of 21 divisions analyzed, peripheral BASL location was correctly predicted [labeled (i) in Fig. 4, D, G, and J, and fig. S9]. In five cases, the predicted and observed BASL positions were slightly discordant [divisions labeled (ii) in Fig. 4G and fig. S9]. Such discrepancies are not surprising given the very simplified assumptions used for making the predictions, such as the new walls acting perfectly uniformly to repel BASL. In the remaining three cases, peripheral BASL was located at the opposite end to that predicted [marked (iii) in Fig. 4J and fig. S9]. These exceptions arise when the daughter P cell has near-bilateral symmetry about a plane perpendicular to the new division wall. For a perfectly symmetrical condition, there can be two locations that are furthest from the new wall, on opposite sides of the cell, so either of these could acquire peripheral BASL. Thus, small stochastic fluctuations may account for peripheral BASL sometimes being localized at the end opposite to that predicted (Fig. 4J).

As a final validation of the model, we used it to simulate entire stomatal lineages by using the initial P cell's geometry (simplified with straight walls), growth parameters, and initial location of peripheral BASL. In many cases, the model could account for both the observed pattern of divisions and location of peripheral BASL over multiple rounds of division (Fig. 4, E and H, and fig. S10). In symmetric cases where peripheral BASL is predicted to be at the opposite corner to that observed, the model predicts the lineage to spiral opposite to the observed direction, as expected (Fig. 4K and fig. S10).

Postmitotic polarity switching provides a simple mechanism by which plant stem cells may generate their own neighborhood while also spacing themselves apart. Although this mechanism does not address all elements of stomatal spacing, such as activation of SPCH during secondary stomata formation, it provides one way of preventing formation of adjacent stomata. In a variant of this mechanism, the stem cell could maintain its character for longer than observed for P cells, generating greater levels of internalization, as observed in the *mute* mutant in which GMCs fail to form (*10*). Polarity switching over longer periods might also underlie the behavior of fern and moss apical cells, which continually generate neighbors around them while maintaining their stem cell identity (*20*–*22*).

Various elements of the polarity switching mechanism are also found for animal stem cells. Polarity of division plays a key role in maintaining animal stem cell identity (*23*). Animal stem cells may also generate their own neighborhoods (niches), as described for the *Drosophila* testis (*24*) and mouse intestine (*25*). However,

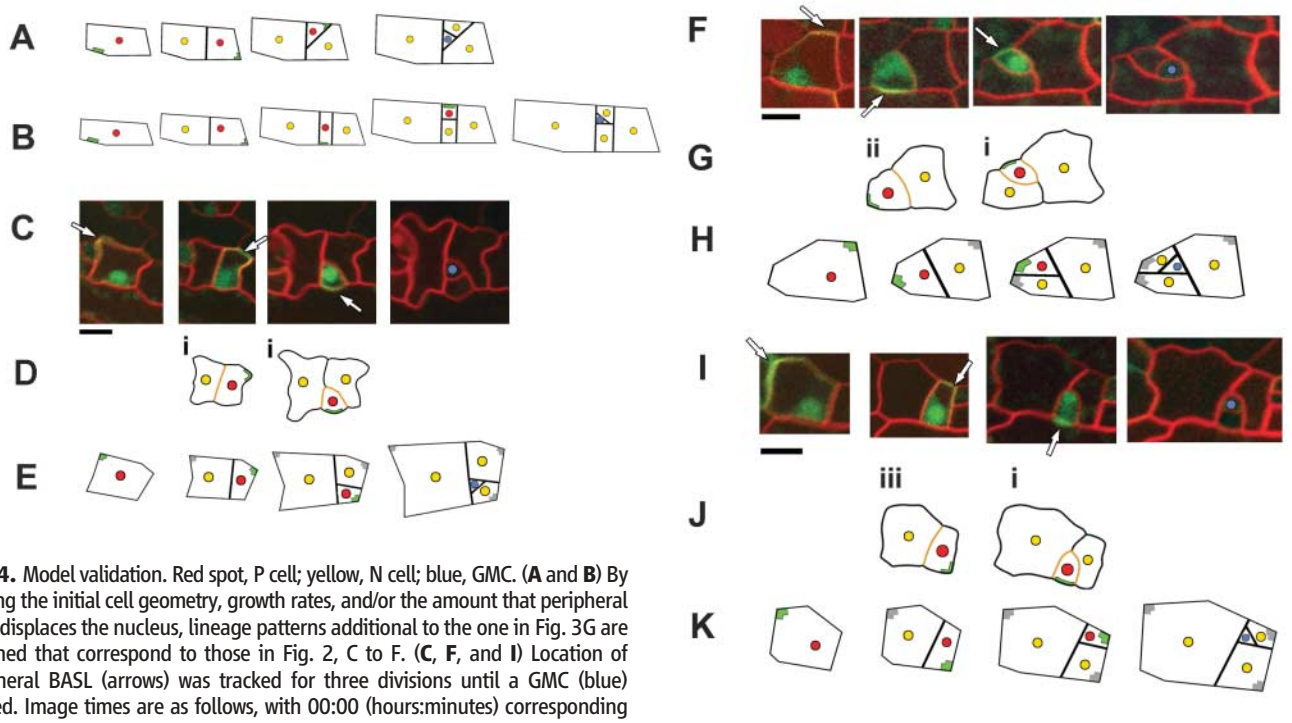

Fig. 4. Model validation. Red spot, P cell; yellow, N cell; blue, GMC. (**A** and **B**) By altering the initial cell geometry, growth rates, and/or the amount that peripheral BASL displaces the nucleus, lineage patterns additional to the one in Fig. 3G are obtained that correspond to those in Fig. 2, C to F. (**C**, **F**, and **I**) Location of peripheral BASL (arrows) was tracked for three divisions until a GMC (blue) formed. Image times are as follows, with 00:00 (hours:minutes) corresponding to the start time: for (C), 00:00, 08:40, 25:20, and 36:00; (F), 00:00, 10:00, 28:00, and 42:40; (I), 00:00, 09:20, 30:00, and 33:20. Scale bars, 10 μm. (**D**, **G**, and **J**) To test the hypothesis that peripheral BASL is located far from new walls (orange), we digitized cell outlines from images and calculated the predicted location of peripheral BASL (green lines). The results are shown below the relevant image. In most cases, the predicted location of peripheral BASL showed a good match to that observed (i); in some cases, the predicted location deviated slightly from that observed (ii); whereas in cases where the cell was approximately symmetric about the new wall, peripheral BASL was sometimes placed on the opposite side to that observed (iii). (**E**, **H**, and **K**) Positions of the original cell vertices were used to drive a growing model, giving an output shown below the relevant images. Observed location of peripheral BASL in the initial image was used as input for the model. The model predicts new wall placement and peripheral BASL locations in daughter cells. Two parameters (extent of nuclear movement and division time) were varied to produce the best fit to the data. In (K) the model produces a lineage spiraling in the opposite direction to that observed because peripheral BASL is placed in the opposite corner in the first division because of symmetry.

unlike stomatal development, cell rearrangements play an important part, so it is unclear whether polarity switching would provide a robust mechanism for patterning in these cases. Thus, although sharing many elements with animal systems, the fixed nature of plant cells may lead to distinctions in the way cells pattern themselves in dynamically changing tissues.

References and Notes

1. T. Sachs, *Pattern Formation in Plant Tissues*, P. W. Barlow, D. Bray, P. B. Geen, J. M. W. Slack, Eds. (Developmental and Cell Biology Series, Cambridge Univ. Press, Cambridge, 1991).
2. M. K. Barton, *Plant Cell* **19**, 1140 (2007).
3. M. Geisler, J. Nadeau, F. D. Sack, *Plant Cell* **12**, 2075 (2000).
4. C. A. MacAlister, K. Ohashi-Ito, D. C. Bergmann, *Nature* **445**, 537 (2007).
5. G. R. Lampard, C. A. Macalister, D. C. Bergmann, *Science* **322**, 1113 (2008).
6. K. Ohashi-Ito, D. C. Bergmann, *Plant Cell* **18**, 2493 (2006).
7. M. M. Kanaoka *et al.*, *Plant Cell* **20**, 1775 (2008).
8. D. Bergmann, *Curr. Opin. Plant Biol.* **7**, 26 (2004).
9. L. B. Lai *et al.*, *Plant Cell* **17**, 2754 (2005).
10. L. J. Pillitteri, D. B. Sloan, N. L. Bogenschutz, K. U. Torii, *Nature* **445**, 501 (2007).
11. J. Dong, C. A. MacAlister, D. C. Bergmann, *Cell* **137**, 1320 (2009).
12. M. T. Fuller, A. C. Spradling, *Science* **316**, 402 (2007).
13. C. van den Berg, V. Willemsen, W. Hage, P. Weisbeek, B. Scheres, *Nature* **378**, 62 (1995).
14. G. J. Mitchison, M. Wilcox, *Nature* **239**, 110 (1972).
15. H. A. Harkins *et al.*, *Mol. Biol. Cell* **12**, 2497 (2001).
16. J. E. Zahner, H. A. Harkins, J. R. Pringle, *Mol. Cell. Biol.* **16**, 1857 (1996).
17. P. H. J. Sahlin, H. Jönsson, *PLoS ONE* **5**, e11750 (2010).
18. L. Errera, *Bot. Centralbl.* **34**, 395 (1888).
19. BASL protein becomes localized in the cell periphery at a position that minimizes the inverse distance from all points along the new division boundaries. See equation in the modeling section of the supporting online material.
20. D. W. Bierhorst, *Am. J. Bot.* **64**, 125 (1977).
21. C. J. Harrison, A. H. K. Roeder, E. M. Meyerowitz, J. A. Langdale, *Curr. Biol.* **19**, 461 (2009).
22. J. Luck, H. B. Luck, *Acta Biotheor.* **43**, 95 (1995).
23. S. E. Siegrist, C. Q. Doe, *Cell* **123**, 1323 (2005).
24. J. Voog, C. D'Alterio, D. L. Jones, *Nature* **454**, 1132 (2008).
25. T. Sato *et al.*, *Nature* **459**, 262 (2009).

Acknowledgments: We thank A. Bangham, G. Calder, S. Fox, S. Sauret-Güeto, and J. Avondo for their help with this work, as well as horticultural services, the media kitchen staff, and computing. This work was funded by the UK Biotechnology and Biological Sciences Research Council (BB/F005997/1), Natural Sciences and Engineering Research Council (Discovery grant 130084), and NIH (1RO1GM086632-02).

Supporting Online Material

www.sciencemag.org/cgi/content/full/333/6048/1436/DC1
Materials and Methods
Figs. S1 to S10
References (*26*–*32*)

27 December 2010; accepted 19 July 2011
10.1126/science.1202185

X-ROS Signaling: Rapid Mechano-Chemo Transduction in Heart

Benjamin L. Prosser,[1] Christopher W. Ward,[2]* W. J. Lederer[1]*

We report that in heart cells, physiologic stretch rapidly activates reduced-form nicotinamide adenine dinucleotide phosphate (NADPH) oxidase 2 (NOX2) to produce reactive oxygen species (ROS) in a process dependent on microtubules (X-ROS signaling). ROS production occurs in the sarcolemmal and t-tubule membranes where NOX2 is located and sensitizes nearby ryanodine receptors (RyRs) in the sarcoplasmic reticulum (SR). This triggers a burst of Ca^{2+} sparks, the elementary Ca^{2+} release events in heart. Although this stretch-dependent "tuning" of RyRs increases Ca^{2+} signaling sensitivity in healthy cardiomyocytes, in disease it enables Ca^{2+} sparks to trigger arrhythmogenic Ca^{2+} waves. In the mouse model of Duchenne muscular dystrophy, hyperactive X-ROS signaling contributes to cardiomyopathy through aberrant Ca^{2+} release from the SR. X-ROS signaling thus provides a mechanistic explanation for the mechanotransduction of Ca^{2+} release in the heart and offers fresh therapeutic possibilities.

In the heart, mechanical stretch during diastolic filling activates mechanotransduction signaling pathways that have broad implications for cardiac health and disease (*1*, *2*). A small diastolic stretch (8%) (*3*) of a ventricular myocyte causes a burst of Ca^{2+} sparks (*4*), the elementary events corresponding to the release of free Ca^{2+} from intracellular stores (Fig. 1, A to C) (*5*, *6*). The mechanism by which this occurs has remained elusive. To address this question, we created tools to improve investigation of single-cell function (Fig. 1A, fig. S2, and movies S1 and S2) (*4*, *7*, *8*). We firmly attached single myocytes to stiff glass micro-rods with a biological adhesive (MyoTak) (*8*). This allows precise control of cell length and the measurement of isometric force, thus permitting us to examine the details of stretch-dependent signal transduction. Such work reveals that stretch-activated Ca^{2+} sparks are triggered by a mechano-chemo signaling pathway that regulates local production of reactive oxygen species (ROS) in heart cells.

Stretching of myocytes initiated a burst of Ca^{2+} sparks that was rapid in onset (milliseconds) and large in magnitude (a nearly twofold increase) (Fig. 1C). Although diastolic stretch in normal myocytes produces the spark burst, under pathological conditions the identical stretch generated transient increases in the intracellular concentration of free Ca^{2+} ($[Ca^{2+}]_i$) that propagate as waves through the cell (Ca^{2+} waves). Such conditions include Ca^{2+} overload of the sarcoplasmic reticulum (SR) (Fig. 1D) and pharmacological sensitization of ryanodine receptors (RyR2s) (fig. S3). Stretch-activated sparks are not influenced by stretch-activated channels, Ca^{2+} influx, Na^+ influx, nitric oxide signaling (*4*), nor acute stretch-induced increases in SR $[Ca^{2+}]$ (*9*). To explore how stretch activates Ca^{2+} signals under normal and pathological conditions, we examined cardiomyocytes from the stretch-sensitive muscular disorder, Duchenne muscular dystrophy (DMD). The frequency of Ca^{2+} waves produced by cellular stretch was increased in cardiomyocytes from the mouse model of DMD, the *mdx* mouse, compared with wild-type (WT) cells (Fig. 1, E and F). Recent reports that ROS-dependent nitrosylation (*10*) and oxidation (*11*, *12*) of RyR2s contribute to aberrant Ca^{2+} release from the SR and arrhythmia in *mdx* myocytes encouraged us to examine ROS signaling.

ROS and reactive nitrogen species (RNS) react with cysteine residues on RyR2 to rapidly and reversibly modulate RyR2 $[Ca^{2+}]_i$ sensitivity (*10*, *13*–*15*). Application of the antioxidant N-acetylcysteine (NAC) to healthy myocytes blocked the stretch-induced burst of Ca^{2+} sparks (Fig. 2A), suggesting that stretch-dependent oxidation of RyR2s (*11*, *14*, *15*) may underlie the increase in spark frequency. To assay whether such a mechanism could account for the rapid changes in Ca^{2+} spark rate observed (Fig. 1C), we superfused cells with 200 μM H_20_2 and assayed spark activity (fig. S4A). Superfusion of H_20_2 reversibly increased Ca^{2+} spark rate, with kinetics and magnitude similar to that observed with physiologic stretch (fig. S4, A to C), confirming that an oxidative mechanism can account for rapid and reversible regulation of RyR2 $[Ca^{2+}]_i$ sensitivity during stretch.

Because NAC indiscriminately scavenges all ROS and reactive nitrogen species (RNS), we sought to identify the specific source of RyR2 oxidation. The reduced-form nicotinamide adenine dinucleotide phosphate (NADPH) oxidase (NOX) family of enzymes represents a major source of ROS in the cardiovascular system (*16*) and has a central role in the pathology of DMD (*12*, *17*) and heart disease (*18*). Unlike other ROS sources (for example, xanthine oxidases,

[1]Center for Biomedical Engineering and Technology (BioMET), University of Maryland School of Medicine, Baltimore, MD 21209, USA. [2]School of Nursing, University of Maryland, Baltimore, MD 21209, USA.

*To whom correspondence should be addressed. E-mail: ward@son.umaryland.edu (C.W.W.); jlederer@umaryland.edu (W.J.L.)